Modelling Coal Dust Explosibility of Khyber Pakhtunkhwa Coal Using Random Forest Algorithm

Amad Ullah Khan [1], Saad Salman [2], Khan Muhammad [2,3,*] and Mudassar Habib [1]

1   Department of Chemical Engineering, University of Engineering and Technology, Peshawar 25000, Pakistan; amadullah@uetpeshawar.edu.pk (A.U.K.); muddasarhabib@uetpeshawar.edu.pk (M.H.)
2   National Centre of Artificial Intelligence, Intelligent Information Processing Laboratory, University of Engineering and Technology, Peshawar 25000, Pakistan; saad_salman@uetpeshawar.edu.pk
3   Department of Mining Engineering, University of Engineering and Technology, Peshawar 25000, Pakistan
*   Correspondence: khan.m@uetpeshawar.edu.pk; Tel.: +92-91-9216796-8 (ext. 3031)

Abstract: Coal dust explosion constitutes a significant hazard in underground coal mines, coal power plants and other industries utilising coal as fuel. Knowledge of the explosion mechanism and the factors causing coal explosions is essential to investigate for the identification of the controlling factors for preventing coal dust explosions and improving safety conditions. However, the underlying mechanism involved in coal dust explosions is rarely studied under Artificial Intelligence (AI) based modelling. Coal from three different regions of Khyber Pakhtunkhwa, Pakistan, was tested for explosibility in 1.2 L Hartmann apparatus under various particle sizes and dust concentrations. First, a random forest algorithm was used to model the relationship between inputs (coal dust particle size, coal concentration and gross calorific value (GCV)), outputs (maximum pressure (P_{max}) and the deflagration index (K_{st})). The model reported an R^2 value of 0.75 and 0.89 for P_{max} and K_{st}. To further understand the impact of each feature causing explosibility, the random forest AI model was further analysed for sensitivity analysis by SHAP (Shapley Additive exPlanations). The study revealed that the most critical parameter affecting the explosibility of coal dust were particle size > GCV > concentration for P_{max} and GCV > Particle size > Concentration for Kst. Mutual interaction SHAP plots of two variables at a time revealed that with <200 gm/L concentration, −73 μm size and a high GCV coal was the most explosive at a high concentration (>400 gm/L), explosibility is relatively lower irrespective of GCV and particle sizes.

Keywords: coal dust explosibility; random forest; SHAP

1. Introduction

The explosion is "an event that once initiated, grows rapidly and initially unbounded" [1]. Therefore, the need for coal dust explosion investigation is a factor for safety in the chemical process industries and its storage for potential energy management [2]. Furthermore, coal dust explosion in a confined environment (coal mine and chemical process industries) results in the production of high pressure due to heating and the expansion of air and gases produced, which leads to destruction and human loss.

Therefore, understanding coal dust explosions is significant to finding the governing factors to mitigate them for increasing safety in industrial working environments. It has been reported that coal dust explosibility is affected by particles size, amount of fines [3], ignition temperature [4,5], air quantity [6] and concentration of coal [7–9] in an explosive environment [10]. The P_{max} (in MPa or bar) indicates the maximum destructive pressure released from a coal dust explosion, and the deflagration index (K_{st} in MPa or bar-m/s) is reported as the measure of explosibility [11]. The strength of explosibility is represented by the K_{st} values from no explosion (0) to weak (0–200), intense (200–300) and powerful (> 300) [12].

Sensors are available to monitor dust concentration and size [13], supported by communication through cloud computing [14]. With the emerging fields of IoT and real-time prediction, e.g., water in-rush [15], tailing dam stability [16], coal fire in sealed off regions [17], and stress monitoring in underground mines [18], available sensors for measuring coal quality, size and dust concentration could be used to predict explosibility as an early warning to prevent explosions. However, apart from other causes such as lack of awareness and safety hazard violations, many coal mining accidents are caused by a lack of calibration of sensors and the non-availability of coal dust prediction systems [19].

In the past few years coal dust explosibility has been studied extensively [5–15]. Coal dust emanates from heavy cutting machines (e.g., longwall mining), crushers and during loading on conveyor belts [20]. The particles may remain suspended where air ventilation velocity is high and later settle on the surface after some time in the accessways and mine entries [21]. The water spray lets the dust settle down, which is powdered with an inert material to reduce its explosibility [22]. Recent trends follow the use of AI to model flame propagation [23] of settled coal dust in galleries. Computational fluid dynamics (CFD) based models have been used to model flame propagation using airflow and coal dust measures [24–27]. Multilinear regression models have been used to model moisture vs. coal explosibility [3]. A generalised model for understanding how different types of explosible coal dust are affected by the coal characteristics and other coal parameters remains a challenge. Rarely has explosibility been modelled using an AI algorithm for investigating various aspects of coal explosibility. Particle dispersion and turbulence [24,28] are vital factors governing dust explosibility, which is dependent on particle concentration, size and shape [26–29]. Therefore, measuring coal dust characteristics during the air suspension phase can enable early monitoring and warning, and it can be an indirect measure to estimate the inert material required after dust suppression. This work is carried out to address the modelling part for its possible subsequent use in these environments in connection with IoT sensors to predict explosibility before time.

The phenomenon of explosibility was modelled using data collected from three different regions of Khyber Pakhtunkhwa (KP) and tested in a 1.2 L Hartman equipment. Using the fractional factorial design, the required number of tests have been conducted to generate data for modelling explosibility by an AI algorithm. A random forest regression algorithm was used to model the effect of coal properties on the response, i.e., the maximum pressure (P_{max}) and the deflagration index (K_{st}). A game theory-based method, Shapley Additive exPlanations (SHAP) [30], explains how the variation in coal dust properties affects the response. Furthermore, sensitivity analysis is performed to quantify this effect and to identify the safe limits for each parameter to mitigate coal explosibility in the KP coal mines.

Literature Review

Many researchers have investigated coal dust explosibility to measure the main factors influencing explosibility [2,4–11,31–34]. Moradi et al. [35] investigated the effect of sizes of coal particles from different mines on the burning rate of coal using a 2-litre closed chamber. The coal dust concentration, pressure and initial temperature were constant at 10000 g/m^3, 1.5 bar and 25 °C, respectively. The response of varying particle sizes was recorded, keeping all the parameters stable. The maximum pressure rate and the explosibility index reported an inverse relationship with the particle size, i.e., 44μm and 37 μm had a higher burning velocity than other dimensions [35]. Another study was conducted on coal dust to measure the explosion severity and the ignition sensitivity of different ranks of coal. Lower ranks of coal are reported to be easily ignited with severe explosion due to the highly volatile content and pyrolytic property of coal [35]. Cao et al. [33] used experimental and numerical analysis to understand the explosion severity of coal dust. The simulations showed the behaviour of coal dust particles after the explosion. These results were consistent with the experimental observations; hence, the simulations can be reliably used to model coal dust explosion. Cashdollar [36] used a US Bureau of Mines (USBM) 20-L laboratory chamber to

measure the effect of coal dust explosibility. The 20-litre chamber data agree relatively well with those from full-scale experimental mine tests.

Particle size, volatile and oxygen [37] contents are almost equally important in governing the strength of coal dust explosibility. Tan et al. [31] used a pipe apparatus to analyse the effect of change in dust particle size, concentration and a mixture of methane-coal dust on the explosion pressure. Both the particle size and the concentrations varied at five different levels. A high explosibility index K_{st} and the maximum pressure P_{max} were recorded for nano-sized particles compared to micro-particles. Similarly, a 38 L explosive chamber was used for testing coal dust explosibility ignition at different concentrations [32]. A 5 KJ Sobbe igniter ignited coal dust to test if the coal was under or over-fueled at different concentrations. It was observed that coal dust concentrations below 100 g/m^3 and 200 g/m^3 failed to deflagrate because of insufficient fuel.

Furthermore, higher dust concentrations above 1200 g/m^3 and 1400 g/m^3 significantly affected the maximum pressure as less oxygen was available to detonate the coal dust sample. When conducting a coal dust explosibility experiment, the range of each parameter plays a vital role in governing the response to the dust explosion. The parameters studied previously with the respective level of variation are reported in Table 1.

Table 1. Ranges of different coal dust parameters in previous research projects.

Sr. No.	Concentration (g/m^3)	Particle Size μm	Volatile Matter (%)	References
1.	213–1282	<38, 38–74, 74–212	17.73	[7]
2.	400,500	5, 11, 33, 95, 145 and 190		[38]
3.	250, 500, 1000, 1500, 2000, 2500, 3000		32.7–44.4	[39]
4.		104-200	Qualitative	[40]
5.	400	20,38,75,250,350		[9]
6.	60, 125, 250, and 500		14.03–40.97	[41]
7.	100 to 600	53, 75	6–38.5	[42]
8.	150, 250, 500	0–56, 56–71 and 71–90		[43]
11.	60, 80, 100, 120, 150, 200, 250, 300, 350, 400, 450 and 500	38,53,73,104,147,300	19.69–27.18	[4]

2. Materials and Methods

2.1. Samples Collection

Three different coal type samples from two regions (Figure 1), i.e., Cherat and Darra localities of KP province in Pakistan, were collected and analysed for the proximate analysis reported in Table 1. After the study, the samples were ground to prepare samples of −43 μm, −53 μm, −75 μm, −120 and +125 μm sizes. The coal particle sizes were tested at concentrations of 50, 100 to 800 gm/L in the 1.2 L Hartmann apparatus. Various particle sizes of coal dust from three different coal types on different concentrations were tested for explosion in the 1.2 L Hartman apparatus and modelled using an RF-based model. This study would help to identify the response parameters, and the sensitivity analysis will help to control coal dust explosions.

**Figure 1.** The regions from which coal samples were collected.

2.2. Experimental Setup

Cerchar first created the Hartman apparatus in the 1970s [44], consisting of a glass tube with a dispersion cup. The powder was dispersed through an air blast and whirled up by the pressurised air. The test substance was then subjected to a flame to determine if it could be ignited by the ignition source [44,45]. The concentration of the dust–air mixture in the Hartmann tube could be varied incrementally between 100 g/m^3 and 4000 g/m^3. Dust could be classified as a dust explosion hazard by this screening if ignition occurred with one of the two ignition types (spark ignition or filament ignition). A complete exclusion of the dust explosion hazard was not possible when screening in the Hartmann tube. Suppose the result of the spark ignition and the filament ignition was negative. In that case, the dust explosion hazard must be examined in the 20 L apparatus in order to make a reliable statement on the dust explosion hazard as stipulated in the standard DIN EN ISO 80079-20-2.

A total of 8 samples, each of 1.5 kg, were collected from the respective sites Dara 1, Dara 2, and Cherat localities. The representative samples from each site were collected, including subsamples using the coning and the quartering method. The samples were crushed in a disc crusher in the Department of Geology, Universiti Teknologi Malaysia (UTM) Johor Bahru. Explosibility tests were conducted in the Explosibility Lab of the Energy Engineering Department UTM Malaysia. The chemical analysis of samples was conducted in the Pakistan Council of Scientific and Industrial Research (PCSIR) Lab Peshawar, Pakistan.

A schematic view of the 1.2 L Hartmann stainless steel tube is presented in Figure 2. An ignition electrode is located on the vertically symmetric axis of the Hartmann tube, approximately 6 inches from the bottom. The minimum ignition energy was the minimum spark energy that could ignite dust and maintain combustion. The ignition source used for the tests is a continuous spark generated by a high voltage transformer between two standardised electrodes placed near the bottom of the cylindrical 1.2 L Hartmann tube. The energy content of the spark corresponds to the equivalent energy of about 10 Joules of

a discharge (temporary) spark. The known concentration and particle size coal sample was placed on an umbellate diffuser arranged in the lower part of the device and used for dust diffusion into a 1.2 L Hartmann tube.
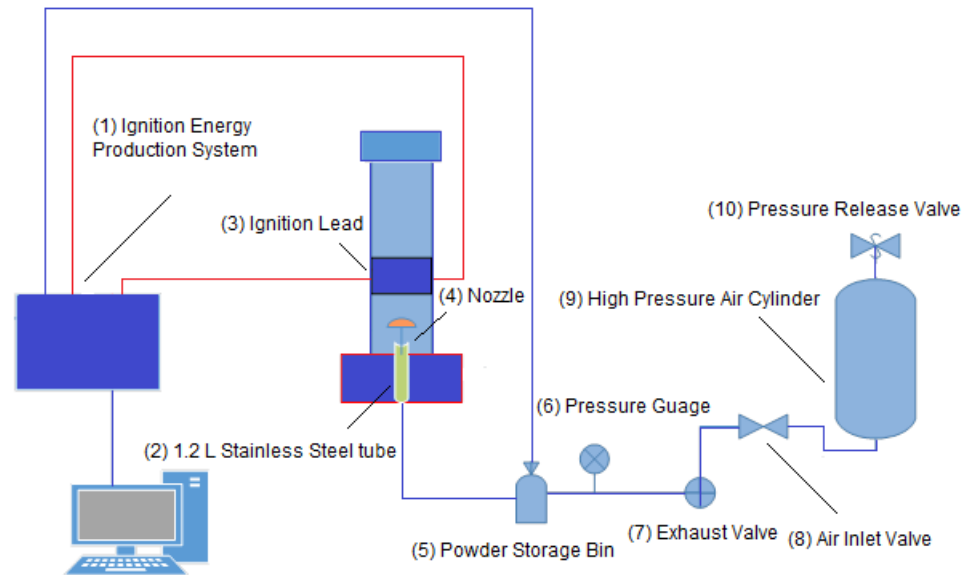
Figure 2. Schematic diagram of the experimental setup for coal dust explosion experiments.

2.3. Random Forest Algorithm

Leo Breiman [46] first proposed the random forest (RF) algorithm as a supervised ensemble learning approach to handle classification and regression tasks. An ensemble learner combines the output from many predictors (trees in this case), referred to as a forest [47], to learn complex relationships. The fundamental unit predictor, i.e., each tree, is obtained by deriving nodes and branches from bootstrapping, using roughly 63% of the original data for training [48]. At the same time, the remaining samples are termed 'out-of-bag' (OOB) samples [49]. Each node in the tree represents the splitting of this training data on an input variable homogeneously, starting from the root node at the top, branching down through subsequent splitting and nodes selection, downward to the leaf (terminal) node representing an output variable. Thus, each node on any tree represents data splitting on a variable recursively down the tree until the terminal node or other stopping criterion is reached. A node variable, i.e., an input variable and a respective cutoff is selected among the 'p' out of 'm' input variables (p < m) and possible cutoff values. A critical trait of RF variable selection during node formation and branching is that the 'p' predictors considered are a subset of 'm' predictors in the bootstrap data, thus resulting in uncorrelated outputs from a collection of B trees termed a forest. Therefore, uncorrelated outputs from each tree in a forest reduces the RF model's variance. For a chosen B possible bootstrapped training data sets, resulting in $b = 1, 2 \ldots B$ trees, a bth bootstrapped training set provide the output $fb(x)$, and finally the average output from all trees report the final estimate

$$fbag\,(x) \;=\; \frac{1}{B} \sum fb(x)$$

Tree building in the random forest regression model commences from the starting node and moves downward using the following steps:

- Divide the predictor space, i.e., the set of all features into J distinct non-overlapping regions $R_1, R_2 \ldots R_j$ (cut values)
- For every observation that falls into a region, make the exact prediction, i.e., the mean of all the response values which fall into that region
- Select the cut value which has the minimum residual sum of squares (RSS)

$$\text{RSS} = \sum_{j=1}^{J} \sum_{i \in R_j} \left(y_i - \hat{y}_{R_j} \right)^2$$

- The same process is repeated at each node until any of the stopping criteria is met Stopping criteria for a regression tree depth can be any of the following:
- Minimum observation at internal node
  - ○ Minimum number of sample observations required for a further split at a node is not met
- Minimum observation at a leaf node
  - ○ Minimum number of sample observations needed is not found at each node after splitting
- Maximum depth of the tree
  - ○ Maximum layers of the tree are reached

When running a machine learning model on any dataset, the variables that govern the model's structure are called hyperparameters. After setting the base model, the hyperparameters need to be tuned to improve the machine learning model's performance. For example, in a random forest regression model, the four primary hyperparameters are as follows:

1. "n_estimators": The number of estimators refers to the number of decision trees built by the random forest regression model before taking the maximum average of predictions. A higher number of trees improve the performance at the cost of computational expense.
2. The "max_depth" maximum depth hyperparameter is the depth of each decision tree in a random forest model. A very high value of the maximum depth hyperparameter leads to overfitting the model.
3. "min_samples_split" is the minimum number of data points placed in a node before splitting the node.
4. "min_samples_leaf" is the minimum number of data points allowed in a leaf node.

2.4. Sensitivity Analysis of the Model

Interpretation of most machine learning models, such as ensemble methods or deep networks, is often complex and commonly referred to as a "black box" [30,50]. In recent times Explainable AI (XAI) algorithms have seen a rising trend, where XAI algorithms like (SHAP, Partial Dependence Plots (PDP), Accumulated Local Effects (ALE), etc.) are used to explain the predictions by AI algorithms [51,52]. SHAP [30] is a novel approach that unveils the learned complexity of these machine learning prediction models. It is a valuable tool for exploring the response of individual variables to output variables as it breaks down the predictions into individual feature impacts [52]. The SHAP feature importance chart reports the importance of each input variable in descending order affecting the output in absolute terms. The feature importance value of an input feature is based on the mean absolute magnitude of the SHAP values over all instances. A summary plot of SHAP values explains the output variable's sensitivity to the concerned input variable. The summary plot can describe the cause-and-effect relationship through high or low values (represented by red to blue colours) of the input feature and the respective SHAP value (of the output) on the horizontal axis. A positive (SHAP value) on the horizontal axis for high values (red) of the input variable refers to a direct relationship while an inverse relationship occurs if the input feature has low (blue) values. In contrast, input features with high values (red) reporting negative (SHAP value) on the horizontal axis would refer to an inverse relationship of the input with the output (response) variable, while a low (blue) value of the input variable would indicate a direct relationship with the output. Jittered points placed densely on the graph represent the same SHAP value reported in numerous instances.

SHAP dependence scatter plots show the effect a feature has on the predictions made by the model. Each point in the scatter plot is a single prediction from the dataset. The

x-axis represents the value of the feature, and the SHAP value on the vertical axis illustrates the effect of a feature's value on the model's output. The colour corresponds to a second feature that interacts with the first feature of concern.

Furthermore, to analyse the outcome of the RF model for the change in each respective input feature, the model was also fed with different values of the feature understudy, holding the mean of all other input features constant.

3. Modelling Explosibility of Coal from Khyber Pakhtunkhwa Province of Pakistan Using Random Forest Regression Model

3.1. Data Collection

The design of experiments is necessary to generate the number of experimental runs with the minimum essential experimentation [53]. The fractional factorial design [54] was used to carry out the experimental runs to investigate these variables' effect on explosibility. Following the design of experiments, different levels of the two input variables, i.e., particle size and concentration, are presented in Table 2. The fractional factorial design suggested 84 runs as an optimal representation of the extent of the full factorial.

Table 2. Coal Types with Proximate Analysis Results.

Coal Type	Total Moisture wt% (Air Dried Basis)	Ash wt%	Volatile Matter wt%	Fixed Carbon wt%	Sulphur wt%	GCV kcal/kg
Cherat	6	26	15.45	49.7	2.81	4901
Dara 1	6.4	17.50	12.26	60.51	3.32	6318.2
Dara 2	7.03	18.57	10.28	61.07	3.02	6120.2

Various concentrations of 0.1, 0.2, 0.3, 0.4, 0.5, 0.6, 0.7, 0.8 and 0.9 g of coal sample were obtained after passing from sieves of the required sizes through disc crusher. Samples were fed to the 1.2 L Hartmann tube and sealed by tightening the screws at the bottom of the tube. Next, the air inlet unit forced compressed air at 15 psi pressure into the air storage tank. Then, a magnetic valve was opened to disperse the coal particles as dust into the tube, followed by the final ignition of the electrode. The pressure sensor transmitted the amplitude of explosion at millisecond intervals for registering values to the LabVIEW software in the personnel computer (PC) connected to the system. The recorded data was used to draw the graphs of pressure change against time to find (dp/dt), for reporting the explosibility (K_{st}). The sensor did not report the dust ignition if the flame propagated less than 60 mm from the spark position; the powder would be considered explosible if the dust fired or exploded during the tests. If no dust fired or exploded in three series of tests for any concentration, the powder was considered not explosible under the test conditions.

The raw data is read from a .csv file with >75,000 readings recorded at milliseconds (ms) interval and plotted against the corresponding pressure (in bar) to determine the maximum slope line (dP/dt) max, i.e., 'maximum rate of pressure rise' (Figure 3). A tangent is fitted to this point and extended to find $dP = (P_{max} - 0)$ and dt, i.e., the difference between times @ P_{max} and intercept at $P = 0$. Finally, the K_{st} values were determined for each test according to the equation given below:

$$K_{st} = \left(\frac{dP}{dt}\right)_{max} V^{\frac{1}{3}}$$
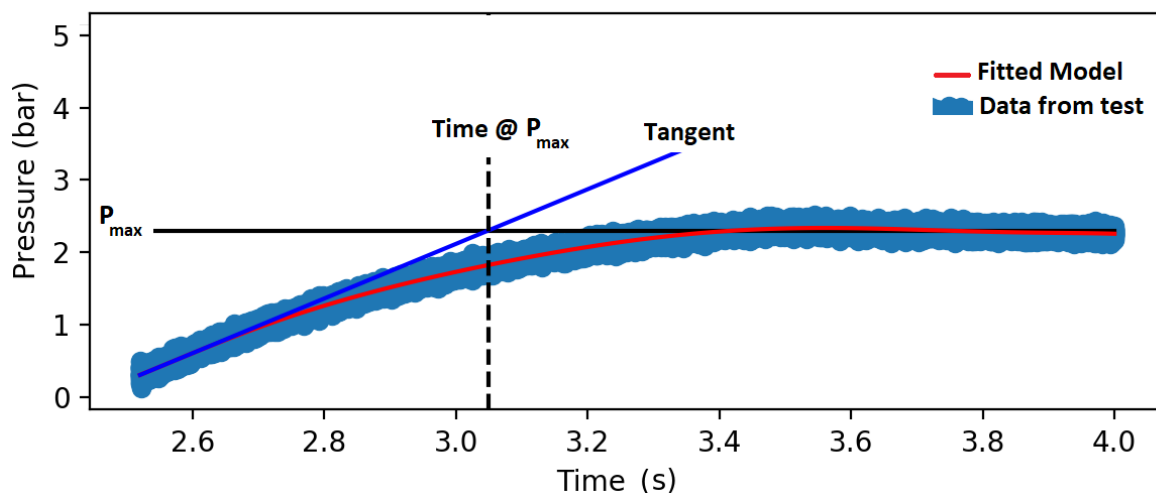
Figure 3. Pressure vs. time and determination of $(dP/dt)_{max}$ for a single explosibility test of 1 gm sample (from Cherat region Khyber Pakhtunkhwa Pakistan) tested in 1.2 L Hartman apparatus with 95 μm size and 500 mg/L concentration.

3.2. Data Preparation

A total of 84 tests were conducted, out of which 81 reported meaningful results. Two samples that reported no explosibility values were removed; one outlier that reported a very high value of K_{st} was also removed. The variables were normalised using the Min–Max scalar to adjust various scales of variables to a standard between 0–1. Principal component analysis (PCA) was applied to sample features reported in Tables 2 and 3, including the outputs P_{max} and K_{st}. Based on selected Eigen loadings (Table 4) of the most critical components defined by Eigenvalues (Table 4), GCV, particle size and concentration were selected. At the same time, redundant features were ignored during further processing. GCV can be considered as an indirect representation of the coal type. Table 5 shows the descriptive statistics of selected features for all 81 samples.

Table 3. Variation of Coal dust concentration and particle size.

Coal Dust Concentration (mg/L)	50	100	200	300	400	500	600	700	800
Size (μm) < (−sign) or >(+sign)	−43	−53	−73	−120	+125				

Table 4. PCA Eigen Vectors and Loadings.

	PC 1	PC 2	PC 3	PC 4	PC 4	PC 5	PC 6	PC 7	PC 8
Eigen Values	182,759.4	63,250.0	519.6	2.7	0.6	0.004	0	0	0
Conc.	−0.0	0.99	0.0	0.0	−0.0	−0.0	0	0	0
size	0.0	−0.0	0.99	0.01	0.01	−0.0	0	0	0
T. Moist	−0.0	0	−0.0	0.2	0.04	−0.0	0.2	0.77	−0.56
Ash	0.0	0	0.0	−0.02	−0.0	0.0	0.6	−0.6	−0.6
V. Matter	0.0	0	0.0	−0.7	−0.2	0.01	−0.5	0.0	−0.5
F. Carbon	−0.0	0	−0.0	0.6	0.14	−0.01	−0.6	−0.3	−0.4
GCV	−0.99	−0.0	0.03	−0.007	−0.001	0.0	0.007	−0.0	−0.0
P_{max}	0.0	−0.0	0.01	0.22	−0.97	−0.14	0	0	0
K_{st}	0.0	−0.0	0.003	0.05	−0.13	0.99	0	0	0

Table 5. Data Descriptive Statistics.

	Concentration mg/L	Particle Size (Micron)	GCV kcal/kg	P_{max} bar	K_{st} bar·m/s
Count	81	81	81	81	81
Mean	405.55	−78.66	6072.73	2.058	0.422
Std dev	251.49	33.42	427.30	0.877	0.165
Min	50	−43	4901	0.15	0.023
Max	800	+125	6318.2	3.41	0.661

Coal dust concentration, particle size and GCV were used as the independent variables and P_{max}, K_{st} as the dependent variables for AI-based modelling. Previously, it was reported that volatile matter is one of the most critical parameters that influence coal dust's explosibility characteristics [34,36]. However, in this case, the range and the magnitude of volatile matter were low (10.28% to 15.45%); therefore, GCV represented a particular coal type. In contrast, the volatile matter content in prior research was 11.19 to 42.26, reporting a more significant effect on the explosibility beyond 20% [34].

The random forest (RF) regression model was applied using the Python Scikit-learn package [55]. The model was trained on 75% of the training data, while the remaining 25% of data was used to test the model accuracy using the train test split method of model selection in sklearn library. To find the best set of hyperparameters of the RF algorithm, the parameters were varied using the grid search CV method [56], as shown in Table 6. A total of 1200 combinations were investigated during hyperparameter tuning.

Table 6. Hyperparameters ranges tried.

S. No	Description	Range	Number of Values
1	"min_samples_split"	2, 3, 4	3
2	"min_samples_leaf"	1, 2, 3, 4	4
3	"n_estimators"	10, 20, 30, 50, 100	5
4	"max_depth"	2, 5, 6, 10	4

$(3 \times 4 \times 5 \times 4) \times 5$ fold cross-validation = 1200 combinations

The 5-fold cross-validation split the data (80:20 train test split ratio) 5 times for each case of the chosen hyperparameters within the grid search and performed the training and testing each time. This hyperparameter tuning process was repeated three times to investigate the effect of random initiation on the hyperparameters. Following the best-chosen hyperparameters based on the grid search, the data was randomly split using the train_test_split method into train:test datasets based on a 70:30 split to train and to test the model. Similarly, the testing accuracy was reported, and the model was further investigated for sensitivity analysis. The most widely used regression evaluation metrics, i.e., coefficient of determination (R^2) [57] and root mean square error (RMSE) [57], were used to evaluate the performance of the RF regression model.

4. Results

Table 7 reports the optimised value for each hyperparameter during the tuning of the model. A Pearson R of 0.86 and 0.94 were observed for the P_{max} and K_{st}, respectively, with the corresponding R^2 of 0.75 and 0.89 for the best combination of hyperparameters (Table 7).

Table 7. Optimised hyperparameters after the Grid search method.

Parameter Name	Description	Value
n_estimators	The number of trees in RF	50
max_depth	The maximum depth of the tree	2
min_samples_leaf	The minimum number of samples required to be at a leaf node	2
min_samples_split	The minimum number of samples required to split an internal node	3

Figure 4 shows the actual vs. the predicted values for both variables. The corresponding root mean square Error (RMSE) were reported as 0.14 and 0.07 for the P_{max} and K_{st} during the testing phase.
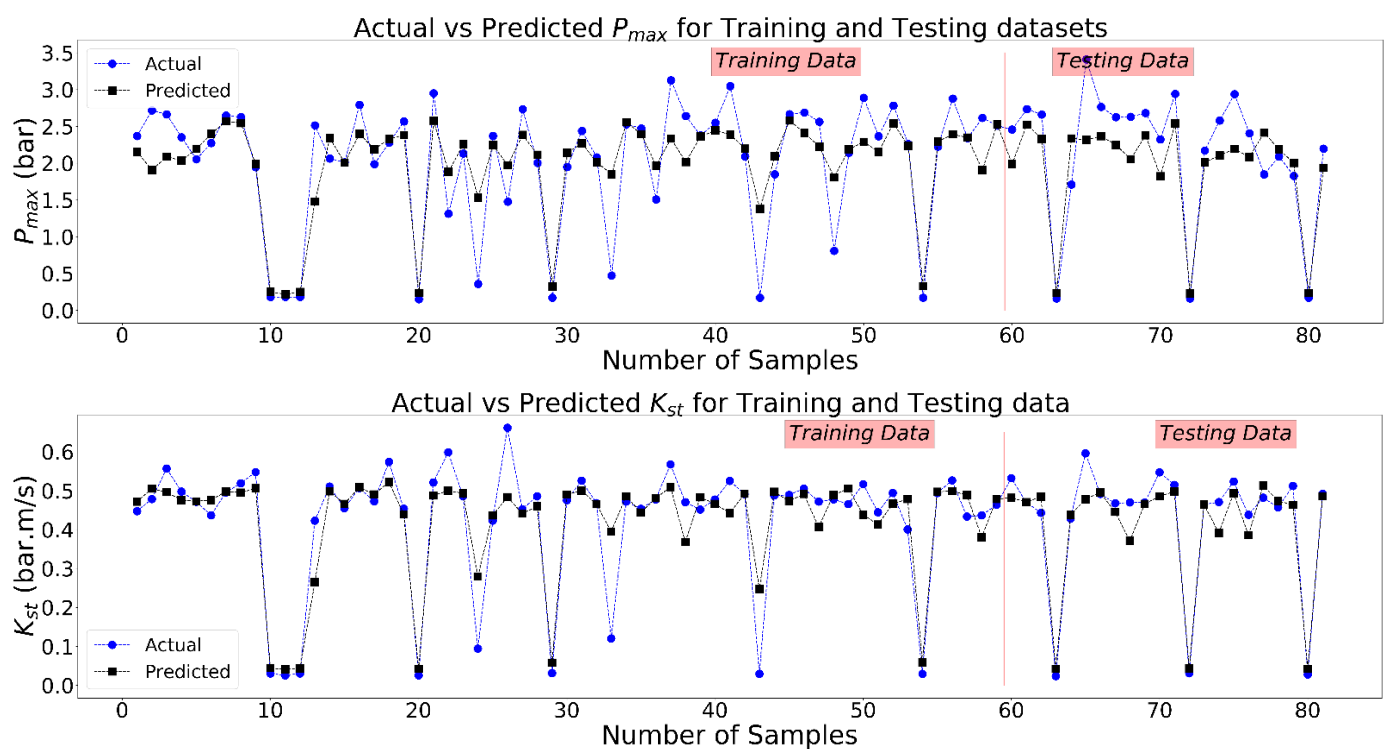
Figure 4. Actual vs. Predicted P_{max} (**top**) and K_{st} (**bottom**) Values.

The magnitude of importance of different input variables was visualised using the SHAP feature importance chart given in Figure 5a,b. The most critical parameter was particle size and GCV for predicting P_{max}, while for K_{st} particle size was the most crucial variable. Observing the SHAP summary plots in Figure 6, concentration indicated an inverse relationship (negative correlation) with P_{max} and K_{st}. Smaller particle sizes reported lower P_{max} and K_{st}, while a mix of different particle sizes caused higher P_{max} and K_{st}, which required further investigation. Similarly, higher GCV coal caused lower or higher P_{max}/K_{st}, while lower GCV coal was positively correlated with P_{max} and K_{st}. Such nonlinear relationships ought to be explored well by the SHAP interaction summary plot given in Figure 7 and the interaction dependence plots in Figure 8 that report the effect of two features on the predicted outcome of a model. It explores if the relationship between the target and the variables is linear, monotonic, or more complex.
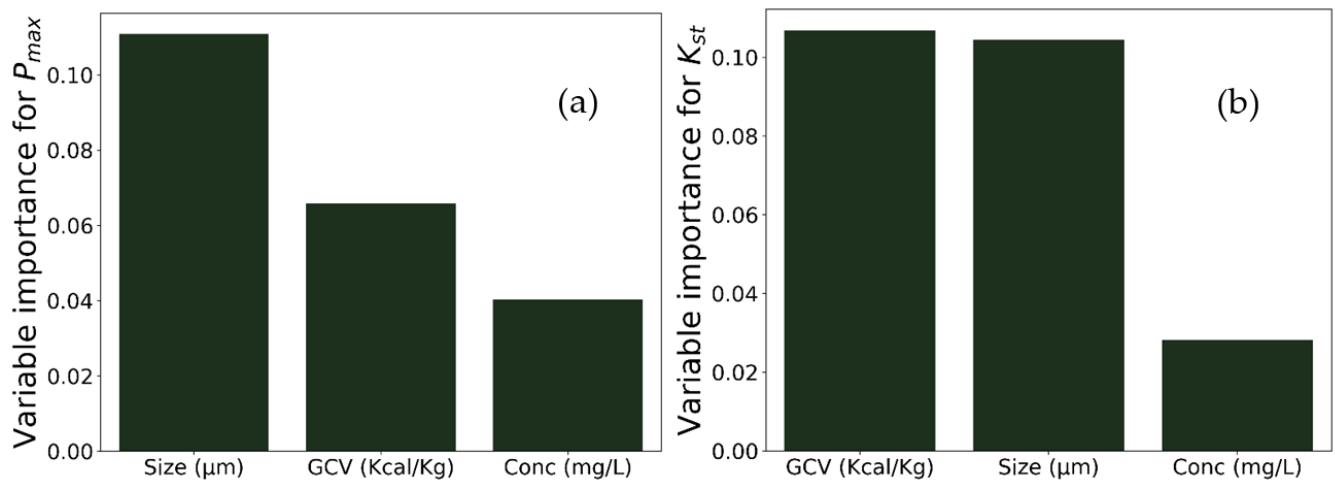
Figure 5. SHAP feature importance chart for (**a**) P_{max} and (**b**) K_{st}.
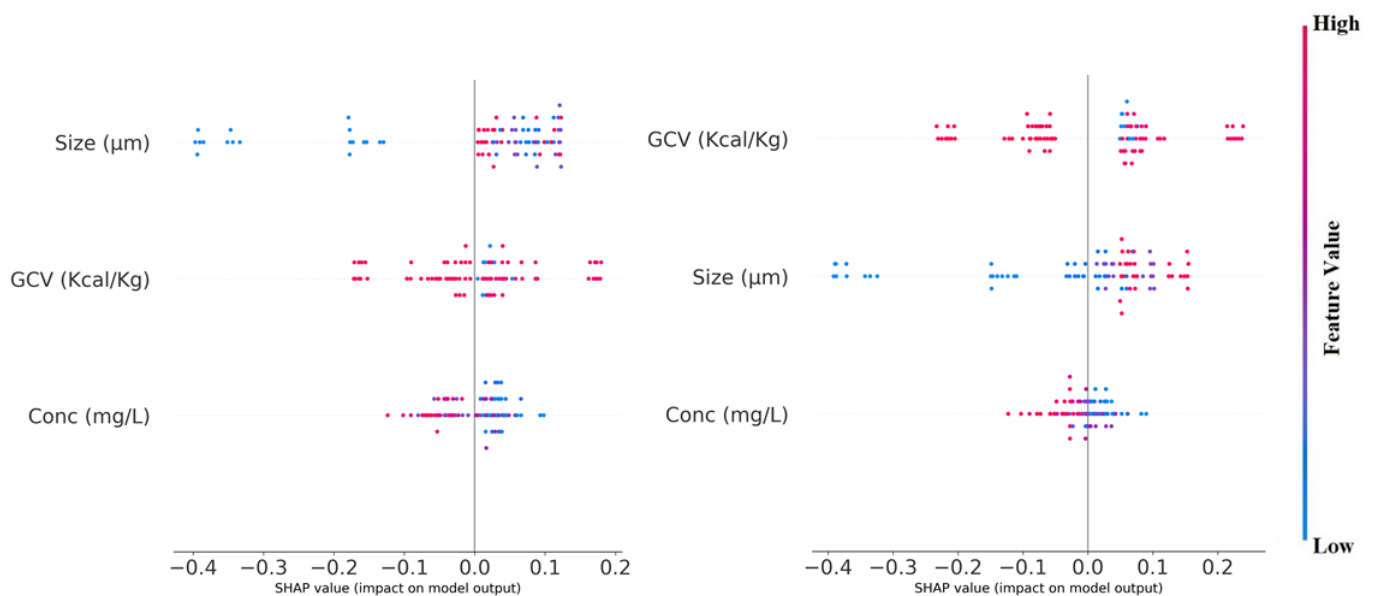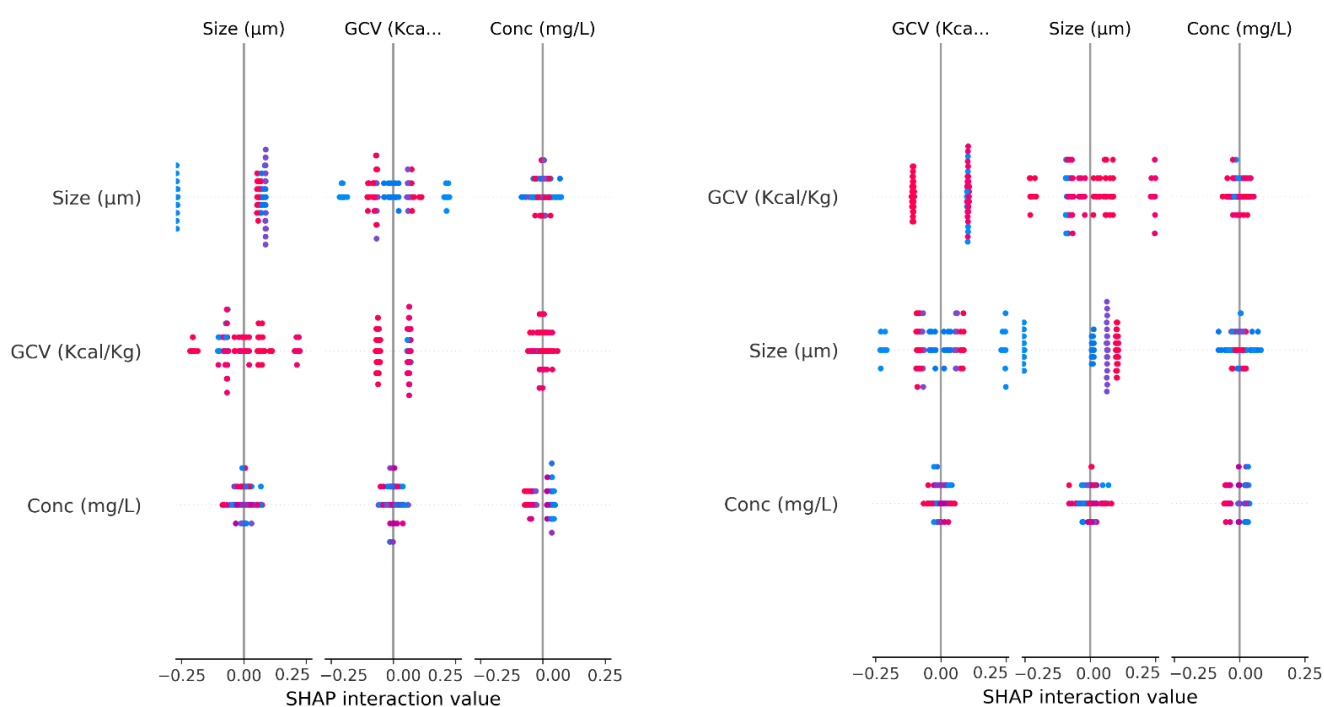

Figure 6. SHAP Summary Plot for P_{max} (**left**) and K_{st} (**right**).

The clearest (and most significant) interaction effect occurs between the size and GCV, indicated by the greatest horizontal spread followed by concentration and size (Figure 7). Conversely, GCV and concentration had a minor interaction. Therefore, to explore further, dependence interaction curves are reported in Figure 8.

Generally, explosibility (K_{st}) decreased with increasing concentration, as seen in Figure 8a. At smaller concentrations, i.e., <200 mg/L, explosibility was higher. Fine sizes, i.e., <−73, had a high positive contribution to K_{st} compared to larger particle sizes (>−73 as red dots), showing a low positive contribution to K_{st} (SHAP values are close to 0). At greater concentration (>500 gm/L), particle sizes <−73 have a higher negative impact on K_{st} than greater particle sizes. Between 300–400 mg/L concentration, the positive impact of K_{st} exists at a lower strength (lower positive SHAP values), as a threshold concentration at which the high impact of coarse particle sizes starts becoming evident and then subsides beyond 500 gm/L concentration. Figure 8c also reports the general decreasing trend of K_{st} with the increase in concentration. Figure 8c,d show that at smaller concentrations (<200 gm/L), higher GCV coal increased explosibility (K_{st}) compared to lower GCV coal which had a minimal effect on explosibility. At 400 gm/L concentration, the overall impact is positive on K_{st}. However, beyond a 400 gm/L concentration, high GCV coal negatively

impacted explosibility (K_{st}), while low GCV coal had nearly no impact on K_{st}. Furthermore, Figure 8d shows that lower GCV (Cherat coal) did not affect explosibility, whereas medium GCV (Darra 2) coal reported higher K_{st}, while lower K_{st} was reported by Darra 2 coal (GCV = 6138). Larger particle sizes increased explosibility (Figure 8e) for even lower GCV Cherat coal. In comparison, medium GCV Darra 2 coal had a minimum effect on explosibility for larger sizes, while fine sizes caused higher explosibility with high positive SHAP values (Figure 8f). Moreover, the higher GCV Darra 1 coal reported the least overall explosibility and a relatively lower explosibility for smaller sizes than larger.

In the case of dependence interaction plots for P_{max}, a decrease in P_{max} is seen with increasing concentration (Figure 9a), similar to Figure 8a. The horizontally opposite Figures complimented each other during interpretation. For example, the value for size is read from Figure 9b, while explaining the concentration interaction with size in Figure 9a. Similarly, interpreting Figure 9b concerning the importance of concentration to size, the concentration values can be read from Figure 9a.


Figure 7. SHAP interaction summary plot of variables for P_{max} (**left**) and K_{st} (**right**).

A nonlinear relationship is shown between concentration vs. size for P_{max}, where at a low concentration (<−200 mg/L), smaller sizes report a highly positive effect on P_{max} (Figure 9a); −53 µm size being the dominating cause of high P_{max}, as seen in Figure 9b. Beyond 500 gm/L concentration, negative SHAP values indicate a higher concentration inverse effect P_{max} irrespective of particle sizes. However, between 400–500 mg/L, larger particle sizes have a higher positive impact on P_{max}, and finer sizes have a lower impact (SHAP values are close to 0). The −43 micron sizes exhibit very low SHAP values, indicating they highly reduce explosibility, as shown in Figure 9b.

The particle size showed an increasing trend for P_{max} beyond −53 µm size in Figure 9b due to the nonlinear concentration vs. size interaction explained in Figure 9a. Figure 9c also showed a decreasing trend of P_{max} with an increase in concentration, as in Figure 9a. In Figure 9c, at higher concentrations, >500 mg/L, a drop is observed in P_{max} for both low and high GCV coal. Figure 9e shows that P_{max} reported an increase as the size increased. Cherat coal (lower GCV) reported a slight positive correlation with P_{max} (Figure 9f), while Darra 2 coal (6120 kcal/kg GCV) had a greater positive P_{max} for smaller particle sizes compared to those that were larger (Figure 9f). The impact of Darra 1 coal (6318 kcal/kg GCV) was

highly negative (inverse) among the coal types. A similar effect was seen for smaller sizes of this coal type than larger sizes.
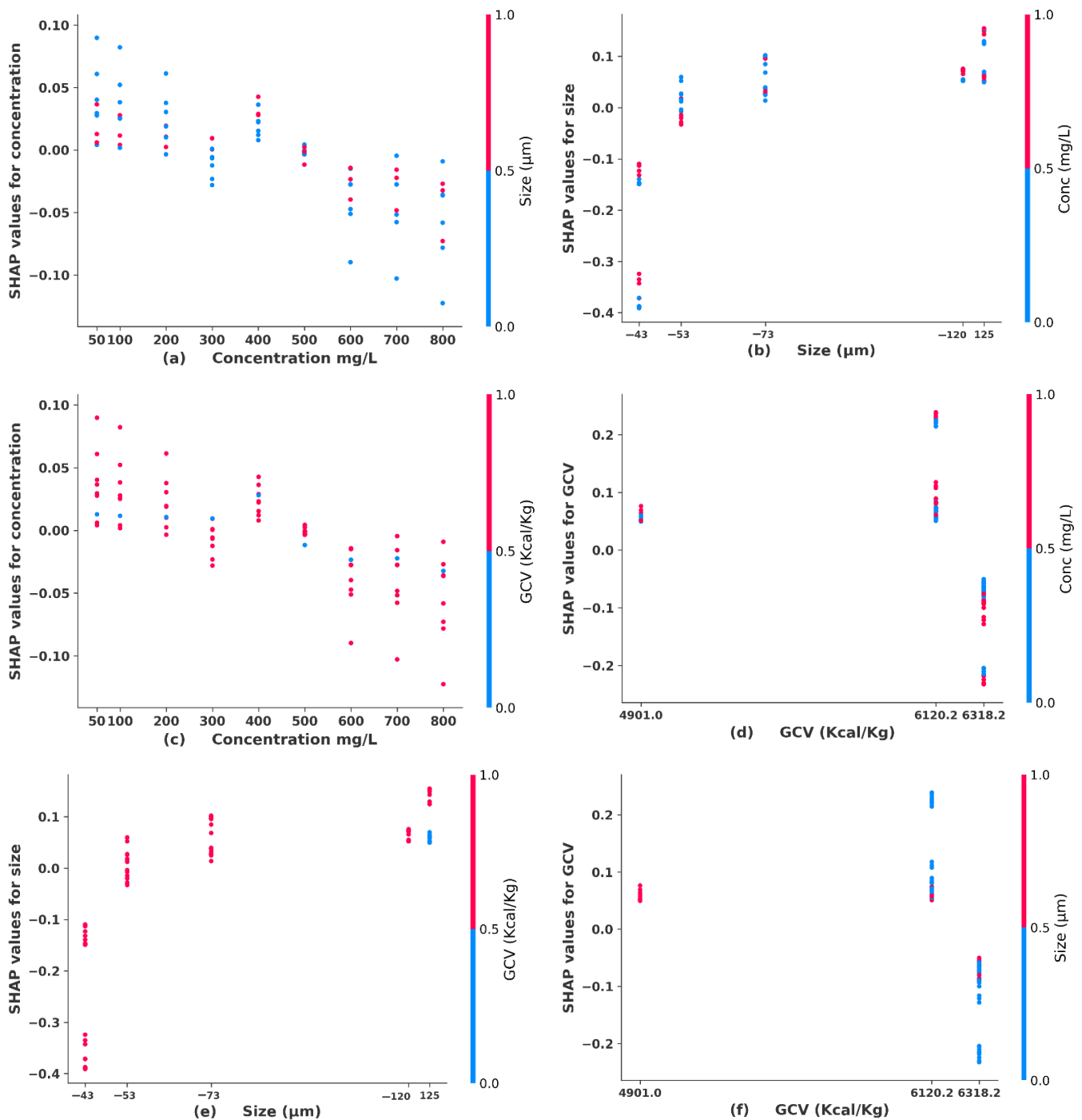
Figure 8. Interaction dependence plots of (**a**) concentration vs. size, (**b**) size vs. concentration, (**c**) concentration vs. GCV, (**d**) GCV vs. concentration, (**e**) size vs. GCV and (**f**) GCV vs. size for K_{st} from SHAP values for explaining the RF model.
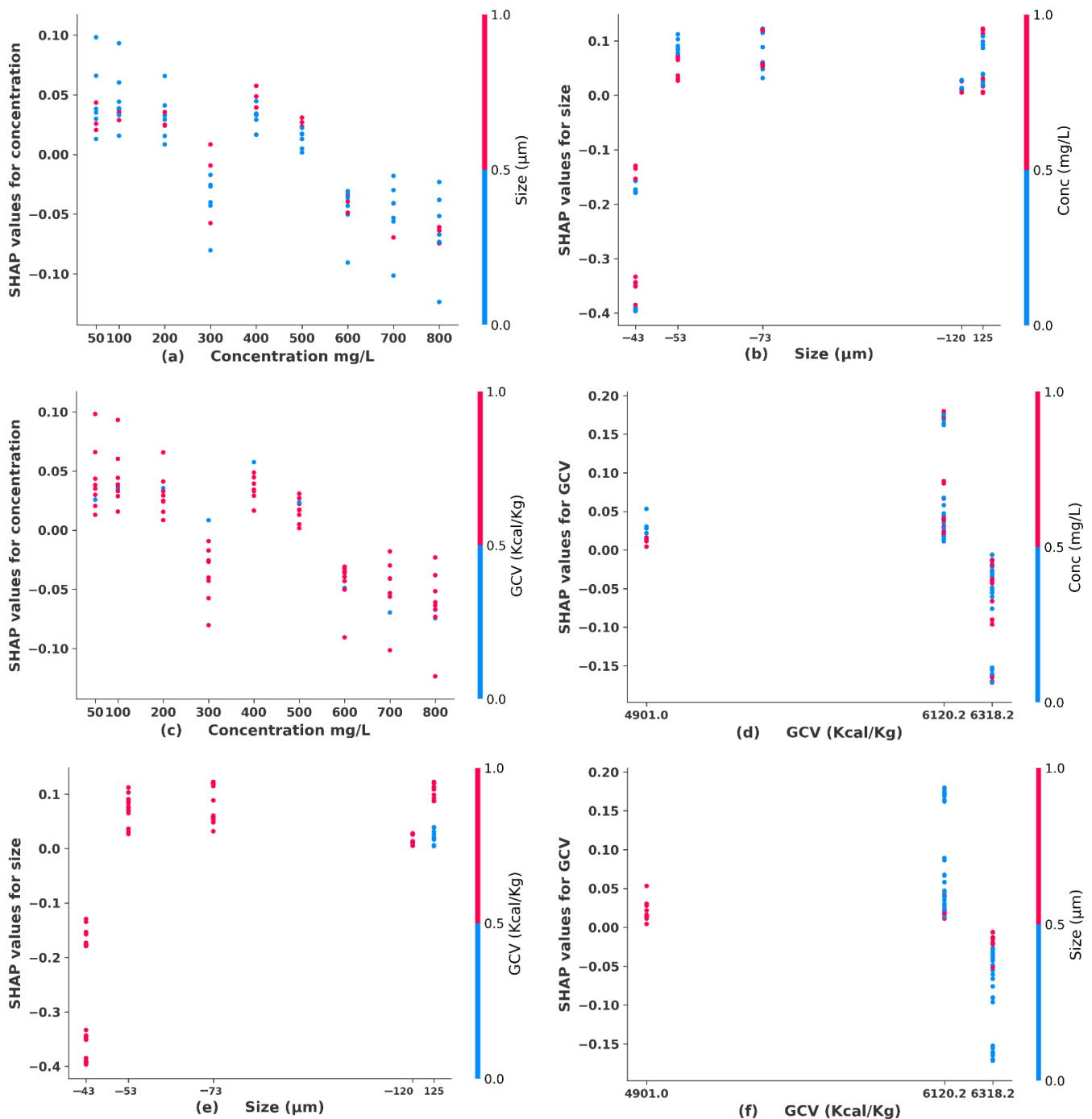
Figure 9. Interaction dependence plots of (**a**) concentration vs. size, (**b**) size vs. concentration, (**c**) concentration vs. GCV, (**d**) GCV vs. concentration, (**e**) size vs. GCV and (**f**) GCV vs. size for P_{max} from SHAP values for explaining the RF model.

To further explore the sensitivity of output variables, one of the input variables (particle size, concentration and GCV) was varied while keeping other input variables constant at the mean values given in Table 5. The results were plotted and reported in Figure 10. Figure 10a,b showed that the P_{max} and K_{st} decreased with increased concentration, as reported in Figure 8a,b. Figure 10c,d indicated that P_{max} and K_{st} increased with particle sizes and dropped beyond −53 microns and −120 microns, respectively. P_{max} and K_{st} are the least for the highest GCV as in Figure 10e,f. These results give similar results to the

SHAP dependence plots, but the SHAP dependence plots are more detailed, highlighting the interaction between two variables.
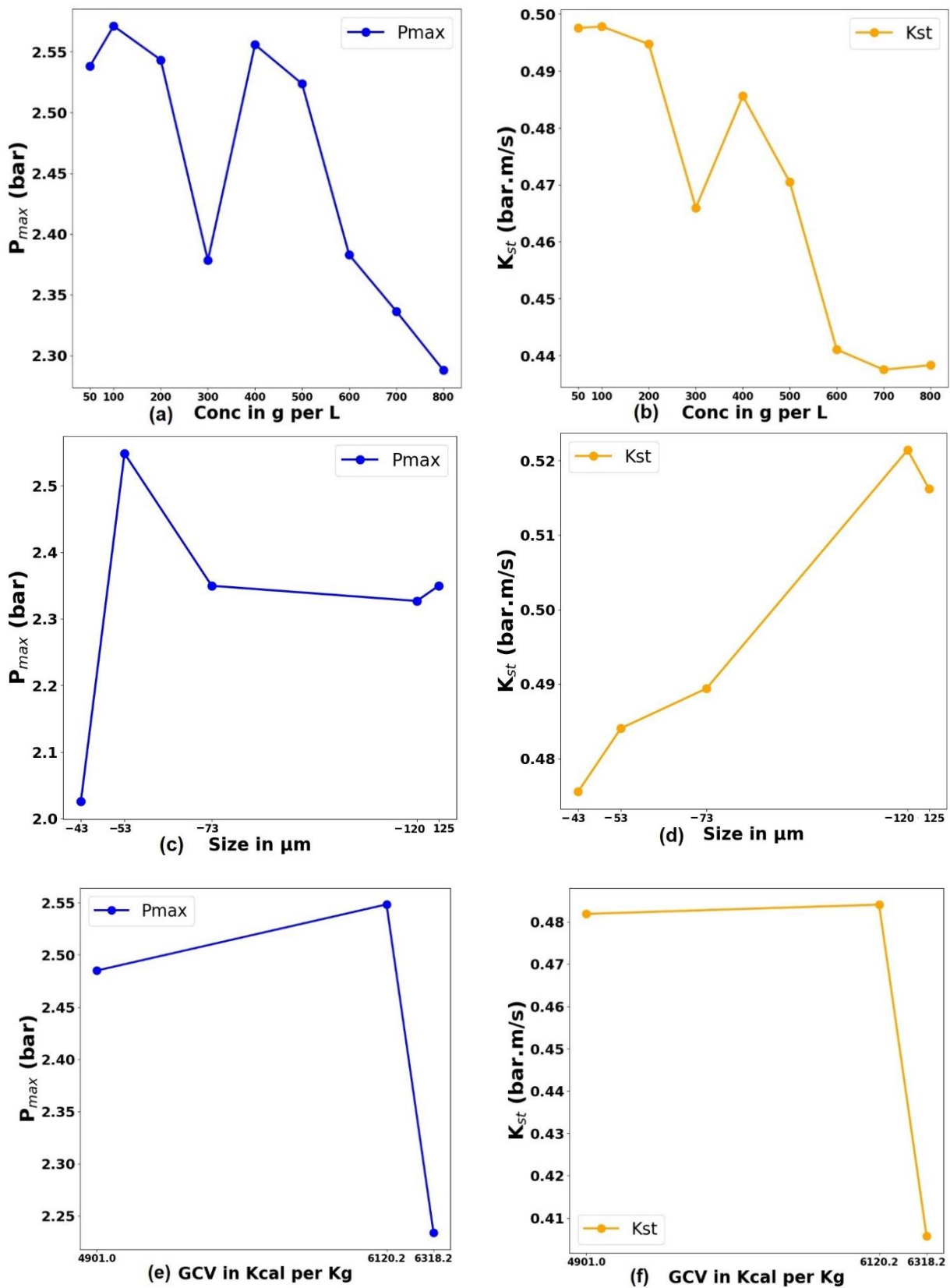

Figure 10. Sensitivity Analysis Graphs for each input variable.

5. Discussion

Machine learning models are considered black-box models that do not explain cause-and-effect relationships. However, SHAP gave some interesting insights into the cause-and-effect relationship between inputs (size, concentration and coal type represented by GCV and outputs (explosibility (K_{st}) and maximum pressure (P_{max})). It is evident from Figure 8a,b,e,f and Figure 9a,b,e,f that different particle sizes of coal dust have a significant effect on both P_{max} and K_{st}. Smaller particle sizes cause smooth and robust deflagration due to greater intermolecular forces [49] and a higher contribution to volatilisation [41]. The model clearly shows this effect at lower concentrations <300 gm/L. Larger particles are relatively dispersed in the form of flakes with edges and corners [31]. However, larger particle sizes exhibited stronger explosibility (K_{st}) and maximum pressure (P_{max}) at medium concentrations (400 gm/L). Moreover, because the particle size ranges -43, -53, -73, and -120 µm were cumulative, there was higher size dispersity as the particle size increased.

Moreover, coal dust lifted by impact airflow has dispersion and sedimentation processes. Therefore, the dispersion and the sedimentation rates of coal dust with different particle sizes are also different, which may have influenced the suspension state of coal powder. In addition, the coal powder was not added with any anti-agglomerating substance; thus, agglomeration may occur in the explosion, thereby influencing the combustion performance of coal dust. Additionally, the +125 µm particle sizes that exclude sizes smaller than this range also report high P_{max} and K_{st} in Figures 8b and 9b. Such an effect may occur if the participation of coal dust in the explosion belonged to a gas–solid reaction; hence, the reaction process and the mechanism may be more complicated.

In this study, higher GCV (6120 and 6318) and small sizes significantly affected both explosibility and the maximum pressure. Dara 1 coal (GCV: 6318) reduces the P_{max} and K_{st} at smaller sizes than a larger size, and Dara 2 coal (GCV: 6120) increases both P_{max} and K_{st} at smaller sizes compared to those that are larger. Additionally, the lower GCV (4901) Cherat coal had minimal effect on P_{max} and K_{st}.

The concentration, in general, has an inverse relationship with both P_{max} and K_{st}, i.e., lower concentration coal has high explosibility and vice versa. This may be because there is sufficient oxygen for combustion reaction at low/medium concentrations or medium carbon content represented by lower or medium GCV, aiding in faster heat transfer [58].

Without oxygen at higher concentrations, the densely concentrated dust particles cannot get enough oxygen molecules to deflate completely. Furthermore, the leftover unreacted molecules absorb the heat, leading to low explosibility [58]. Therefore, a lower explosibility zone is mainly associated with high concentration (>500 mg/L). These results indicate that the oxygen fuel is deficient in higher concentrations (>500 gm/L), causing lower P_{max} and K_{st}; therefore, the 1.2 L Hartmann is limited generally for conducting tests at higher concentrations. It is also observed that smaller particle sizes at lower concentrations are more explosible, i.e., positively contribute to K_{st} and P_{max}, but this effect is reversed at higher concentrations, i.e., smaller particle sizes negatively impacted P_{max} and K_{st}. Additionally, the larger particle sizes showed a minimal impact on explosibility with rising concentrations as they have low SHAP values.

Sensor deployment, supported by the proposed AI model, may be implemented in zones of high air velocities [19], where dust is in suspension with ample oxygen supply. This safety monitoring system may be deployed with other dust suppression/control measures that must also be in place to suppress dust. At 400 to 800 gm/L, the experiments were more dominating due to the lower oxy-fuel ratio; therefore, further experiments at these ranges must be conducted in a 20 L or 1 m^3 chamber to explore explosibility characteristics at these concentrations. An IoT sensor system + AI-based explosibility model may be analysed using coal dust concentration, dust particle size, and coal type parameter as a monitoring and warning system to further this research. The quantity of coal dust concentration and suppression can also be linked to estimating the amount of inert material required to reduce the explosive properties of coal to a safe level.

6. Conclusions

The objective of the work was to address the knowledge gap by AI-based modelling to investigate the effect of coal concentration, coal type and particle size on explosibility K_{st} and P_{max}. Coal from three different localities was tested in 84 experiments to measure the maximum pressure P_{max} and the explosibility index K_{st} in the 1.2 L Hartman apparatus for various concentrations and particle sizes. K_{st} were determined by fitting a tangent to each curve of the experimental run. Samples were recorded for GCV, dust concentration and particle size as input variables to predict P_{max} and K_{st}. The random forest algorithm was applied to the input data for modelling the outputs, reporting R^2 scores of 0.75 and 0.89 for P_{max} and K_{st}, respectively. The Shapley Additive exPlanations (SHAP) algorithm explained the behaviour/prediction of the random forest model, identifying the essential input variable with a sensitive limit. A SHAP based summary plot and interaction dependence curves were plotted to get an insight into the cause-and-effect relationship learned by the model. Additionally, the model's response to the change in each feature was derived through sensitivity analysis, where each feature was varied at different levels. At the same time, all the other components were held constant at the mean values of each respective feature.

The following are the essential conclusions:

- The coal dust samples of the KP region have low volatile matter (10–16%); hence GCV was more representative of coal type as reported by PCA results.
- Initially, SHAP plots reported the parameters influencing the coal dust explosibility in descending order were particle size > GCV > concentration for P_{max} and GCV > particle size > Concentration for K_{st}.
- SHAP plots reliably interpreted the random forest explosibility model explaining the complex inter variable phenomenon in greater detail.
- A SHAP interaction plot revealed that the concentration of coal dust particles has an inverse relationship with P_{max} and K_{st}. A lower concentration results in a higher P_{max} and K_{st}, which is a consequence of sufficient oxygen available to deflagrate all the coal dust particles. High GCV coal is utilised to its maximum at lower concentrations, causing higher explosibility.
- At higher concentrations, there is not enough oxygen for the complete reaction of the coal dust particles. The excess molecules absorb the heat of coal dust explosion, resulting in an overall drop in maximum pressure and explosibility.
- At concentration <200 gm/L, lower particle size (−73 μm) and high GCV coal have the highest explosibility, and more significant particle sizes have no impact.
- 400 gm/L is a threshold concentration as a high impact of fine particle sizes exists, and explosibility is also positively related to this concentration.
- At greater concentrations (>500 gm/L), particle sizes <−73 μm negatively impact K_{st} and P_{max} compared to more significant particle sizes for even lower GCV coal.
- The increase in concentration beyond 400 gm/L decreased explosibility, high GCV coal caused a negative impact on explosibility.
- Concentration vs. size interaction plot showed that lower concentration (<200 gm/L) and fine size (<−73 μm) reported higher P_{max}. While at >500 gm/L concentration, P_{max} decreased irrespective of particle sizes.
- At concentrations between 400–500 mg/L, larger particle sizes positively correlate with P_{max} compared to finer sizes.
- Cherat coal (lower GCV) reported a slight positive correlation with P_{max}, while Darra 2 coal (6120 kcal/kg GCV) had a greater positive P_{max} for smaller particle sizes than those that were larger.
- The impact of Darra 1 coal (6318 kcal/kg GCV) was highly negative (inverse) among the coal types; a similar effect was observed for smaller sizes of this coal type than larger sizes.
- The model is valid for access airway vicinities with high air velocities, where dust is suspended at a lower concentration with ample oxygen supply.

- Further explosibility experiments must be conducted at higher concentrations (400 to 800 gm/L) in a 20 L or 1 m^3 chamber to overcome the lower oxy-fuel ratio within the Hartmann apparatus. These will benefit modelling explosibility in regions of high dust concentrations, e.g., underground mines with medium/lower air velocity.
- An IoT sensor system may be developed by deploying the AI-based explosibility model to use coal dust concentration, particle size, and coal type parameters as a monitoring and warning system.

References

1. Keller, J.O.; Gresho, M.; Harris, A.; Tchouvelev, A.V. What is an explosion? *Int. J. Hydrog. Energy* **2014**, *39*, 20426–20433. [CrossRef]
2. Rice, G.S. *Explosibility of Coal Dust*; USGS Bulletin, Govt. Printing Office: Washington, WA, USA, 1910; Volume 425.
3. Moradi, H.; Sereshki, F.; Ataei, M.; Nazari, M. Evaluation of the effect of the moisture content of coal dust on the prediction of the coal dust explosion index. *Rud. Geol. Naft. Zb.* **2020**, *35*, 37–47. [CrossRef]
4. Mittal, M. Limiting oxygen concentration for coal dusts for explosion hazard analysis and safety. *J. Loss Prev. Process Ind.* **2013**, *26*, 1106–1112. [CrossRef]
5. Gou, X.; Wu, J.; Liu, L.; Wang, E.; Zhou, J.; Liu, J.; Cen, K. Study on factors influencing pulverized coal ignition time. *Adv. Mater. Res.* **2013**, *614–615*, 120–125. [CrossRef]
6. Gokhale, A. Effect of Particle-Size and Air Flow Rates on the Ignition Temperature of Sub Bituminous Coal. *Int. J. Mod. Trends Eng. Res.* **2016**, *3*, 89–97. [CrossRef]
7. Azam, S.; Mishra, D.P. Effects of particle size, dust concentration and dust-dispersion-air pressure on rock dust inertant requirement for coal dust explosion suppression in underground coal mines. *Process Saf. Environ. Prot.* **2019**, *126*, 35–43. [CrossRef]
8. Liu, Q.; Bai, C.; Li, X.; Jiang, L.; Dai, W. Coal dust/air explosions in a large-scale tube. *Fuel* **2010**, *89*, 329–335. [CrossRef]
9. Harris, M.L.; Sapko, M.J.; Zlochower, I.A.; Perera, I.E.; Weiss, E.S. Particle size and surface area effects on explosibility using a 20-L chamber. *J. Loss Prev. Process Ind.* **2015**, *37*, 33–38. [CrossRef]
10. Rybak, W.; Moroń, W.; Ferens, W. Dust ignition characteristics of different coal ranks, biomass and solid waste. *Fuel* **2019**, *237*, 606–618. [CrossRef]
11. Reyes, O.J.; Patel, S.J.; Mannan, M.S. Quantitative structure property relationship studies for predicting dust explosibility characteristics (Kst, Pmax) of organic chemical dusts. *Ind. Eng. Chem. Res.* **2011**, *50*, 2373–2379. [CrossRef]
12. Kazmi, M.Z. Experimental Study of Polyethylene and Sulfur Dust Explosion Characteristics. Master's Thesis, Texas A&M University, College Station, TX, USA, 2018.
13. Lebecki, K.; Małachowski, M.; Sołtysiak, T. Continuous dust monitoring in headings in underground coal mines. *J. Sustain. Min.* **2016**, *15*, 125–132. [CrossRef]
14. Zou, Z.; Zheng, L.; Huang, J.; Li, J.; Wang, J. Design and Implementation of Coal Mine Dust Monitoring System Based on Cloud Platform. In Proceedings of the CSAE '18: 2nd International Conference on Computer Science and Application Engineering, Hohhot, China, 22–24 October 2018; Volume 31, pp. 1–8.
15. Ma, K.; Sun, X.Y.; Tang, C.A.; Wang, S.J.; Yuan, F.Z.; Peng, Y.L.; Liu, K. An early warning method for water inrush in Dongjiahe coal mine based on microseismic moment tensor. *J. Cent. South Univ.* **2020**, *27*, 3133–3148. [CrossRef]

16. Dong, L.; Shu, W.; Sun, D.; Li, X.; Zhang, L. Pre-Alarm System Based on Real-Time Monitoring and Numerical Simulation Using Internet of Things and Cloud Computing for Tailings Dam in Mines. *IEEE Access* **2017**, *5*, 21080–21089. [CrossRef]

17. Kumari, K.; Dey, P.; Kumar, C.; Pandit, D.; Mishra, S.S.; Kisku, V.; Chaulya, S.K.; Ray, S.K.; Prasad, G.M. UMAP and LSTM based fire status and explosibility prediction for sealed-off area in underground coal mine. *Process Saf. Environ. Prot.* **2021**, *146*, 837–852. [CrossRef]

18. Dong, L.J.; Tang, Z.; Li, X.B.; Chen, Y.C.; Xue, J.C. Discrimination of mining microseismic events and blasts using convolutional neural networks and original waveform. *J. Cent. South Univ.* **2020**, *27*, 3078–3089. [CrossRef]

19. Li, X.; Cao, Z.; Xu, Y. Characteristics and trends of coal mine safety development. *Energy Sources Part A Recovery Util. Environ. Eff.* **2020**, 1–19. [CrossRef]

20. Brodny, J.; Tutak, M. Exposure to harmful dusts on fully powered longwall coal mines in Poland. *Int. J. Environ. Res. Public Health* **2018**, *15*, 1846. [CrossRef]

21. Shahan, M.R.; Seaman, C.E.; Beck, T.W.; Colinet, J.F.; Mischler, S.E. Characterization of airborne float coal dust emitted during continuous mining, longwall mining and belt transport. *Min. Eng.* **2017**, *69*, 61–66. [CrossRef]

22. Zlochower, I.A.; Sapko, M.J.; Perera, I.E.; Brown, C.B.; Harris, M.L.; Rayyan, N.S. Influence of specific surface area on coal dust explosibility using the 20-L chamber. *J. Loss Prev. Process Ind.* **2018**, *54*, 103–109. [CrossRef]

23. Liu, T.; Cai, Z.; Wang, N.; Jia, R.; Tian, W. Prediction Method of Coal Dust Explosion Flame Propagation Characteristics Based on Principal Component Analysis and BP Neural Network. *Math. Probl. Eng.* **2022**, *2022*, 1–8. [CrossRef]

24. Di Benedetto, A.; Russo, P.; Sanchirico, R.; Di Sarli, V. CFD Simulations of Turbulent Fluid Flow and Dust Dispersion in the 20 Liter Explosion Vessel. *AIChE J.* **2013**, *59*, 2485–2496. [CrossRef]

25. Di Sarli, V.; Russo, P.; Sanchirico, R.; Di Benedetto, A. CFD simulations of the effect of dust diameter on the dispersion in the 20 l bomb. *Chem. Eng. Trans.* **2013**, *31*, 727–732. [CrossRef]

26. Di Sarli, V.; Danzi, E.; Marmo, L.; Sanchirico, R.; Di Benedetto, A. CFD simulation of turbulent flow field, feeding and dispersion of non-spherical dust particles in the standard 20 L sphere. *J. Loss Prev. Process Ind.* **2019**, *62*, 103983. [CrossRef]

27. Di Sarli, V.; Russo, P.; Sanchirico, R.; Di Benedetto, A. CFD simulations of dust dispersion in the 20 L vessel: Effect of nominal dust concentration. *J. Loss Prev. Process Ind.* **2014**, *27*, 8–12. [CrossRef]

28. Yueze, L.; Akhtar, S.; Sasmito, A.P.; Kurnia, J.C. Prediction of air flow, methane, and coal dust dispersion in a room and pillar mining face. *Int. J. Min. Sci. Technol.* **2017**, *27*, 657–662. [CrossRef]

29. Sanchirico, R.; Russo, P.; Di Sarli, V.; Di Benedetto, A. On the explosion and flammability behavior of mixtures of combustible dusts. *Process Saf. Environ. Prot.* **2015**, *94*, 410–419. [CrossRef]

30. Lundberg, S.M.; Lee, S.I. A unified approach to interpreting model predictions. *Adv. Neural Inf. Process. Syst.* **2017**, *30*, 4766–4775.

31. Tan, B.; Liu, H.; Xu, B.; Wang, T. Comparative study of the explosion pressure characteristics of micro- and nano-sized coal dust and methane–coal dust mixtures in a pipe. *Int. J. Coal Sci. Technol.* **2020**, *7*, 68–78. [CrossRef]

32. Eades, R.; Perry, K. Evaluation of a 38 L Explosive Chamber for Testing Coal Dust Explosibility. *J. Combust.* **2019**, *2019*, 5810173. [CrossRef]

33. Cao, W.; Qin, Q.; Cao, W.; Lan, Y.; Chen, T.; Xu, S.; Cao, X. Experimental and numerical studies on the explosion severities of coal dust/air mixtures in a 20-L spherical vessel. *Powder Technol.* **2017**, *310*, 17–23. [CrossRef]

34. Wang, J.; Meng, X.; Zhang, Y.; Chen, H.; Liu, B. Experimental Study on the Ignition Sensitivity and Explosion Severity of Different Ranks of Coal Dust. *Shock Vib.* **2019**, *2019*, 2763907. [CrossRef]

35. Moradi, H.; Sereshki, F.; Ataei, M.; Nazari, M. Experimental study of the effects of coal dust particle size on laminar burning velocity in a mixture of coal dust and methane. *Min.-Geol.-Pet. Eng. Bull.* **2019**, *34*, 47–56. [CrossRef]

36. Cashdollar, K.L. Coal dust explosibility. *J. Loss Prev. Process Ind.* **1996**, *9*, 65–76. [CrossRef]

37. Song, T.; Zhang, J.; Wang, G.; Wang, H.; Xu, R. Influencing factors of the explosion characteristics of modified coal used for blast furnace injection. *Powder Technol.* **2019**, *353*, 171–177. [CrossRef]

38. Liu, S.H.; Cheng, Y.F.; Meng, X.R.; Ma, H.H.; Song, S.X.; Liu, W.J.; Shen, Z.W. Influence of particle size polydispersity on coal dust explosibility. *J. Loss Prev. Process Ind.* **2018**, *56*, 444–450. [CrossRef]

39. Moroń, W.; Ferens, W.; Czajka, K.M. Explosion of different ranks coal dust in oxy-fuel atmosphere. *Fuel Process. Technol.* **2016**, *148*, 388–394. [CrossRef]

40. Sapko, M.J.; Cashdollar, K.L.; Green, G.M. Coal dust particle size survey of US mines. *J. Loss Prev. Process Ind.* **2007**, *20*, 616–620. [CrossRef]

41. Li, Q.; Wang, K.; Zheng, Y.; Ruan, M.; Mei, X.; Lin, B. Experimental research of particle size and size dispersity on the explosibility characteristics of coal dust. *Powder Technol.* **2016**, *292*, 290–297. [CrossRef]

42. Man, C.K.; Gibbins, J.R. Factors affecting coal particle ignition under oxyfuel combustion atmospheres. *Fuel* **2011**, *90*, 294–304. [CrossRef]

43. Kuracina, R.; Szabová, Z. The Maximum Explosion Pressure of Lignite in Dependence on Particle Size. *Res. Pap. Fac. Mater. Sci. Technol. Slovak Univ. Technol.* **2019**, *27*, 57–64. [CrossRef]

44. Janes, A.; Chaineaux, J.; Carson, D.; Le Lore, P.A. MIKE 3 versus HARTMANN apparatus: Comparison of measured minimum ignition energy (MIE). *J. Hazard. Mater.* **2008**, *152*, 32–39. [CrossRef] [PubMed]

45. Danzi, E.; Franchini, F.; Dufaud, O.; Pietraccini, M.; Marmo, L. Investigation of the fluid dynamic of the modified hartmanntube equipment by high-speed video processing. *Chem. Eng. Trans.* **2021**, *86*, 367–372. [CrossRef]

46. Breiman, L. Random forests. *Mach. Learn.* **2001**, *45*, 5–32. [CrossRef]

47. Efron, B. Bootstrap Methods: Another Look at the Jackknife. In *Breakthroughs in Statistics*; Springer Series in Statistics; Kotz, S., Johnson, N.L., Eds.; Springer: New York, NY, USA, 1992; pp. 569–593.

48. Dasgupta, A.; Sun, Y.V.; König, I.R.; Bailey-Wilson, J.E.; Malley, J.D. Brief review of regression-based and machine learning methods in genetic epidemiology: The Genetic Analysis Workshop 17 experience. *Genet. Epidemiol.* **2011**, *35*, 5–11. [CrossRef] [PubMed]

49. Bu, Y.; Li, C.; Amyotte, P.; Yuan, W.; Yuan, C.; Li, G. Moderation of Al dust explosions by micro- and nano-sized Al_2O_3powder. *J. Hazard. Mater.* **2020**, *381*, 120968. [CrossRef]

50. Bataineh, M.; Steenhard, D.; Singh, H. Feature Impact for Prediction Explanation. In Proceedings of the 19th Industrial Conference on Data Mining, New York, NY, USA, 17–21 July 2019; pp. 160–167.

51. Zou, J.; Petrosian, O. Explainable AI: Using shapley value to explain complex anomaly detection ML-based systems. *Front. Artif. Intell. Appl.* **2020**, *332*, 152–164. [CrossRef]

52. Wieland, R.; Lakes, T.; Nendel, C. Using SHAP to interpret XGBoost predictions of grassland degradation in Xilingol, China. *Geosci. Model Dev. Discuss.* **2020**, 1–28. [CrossRef]

53. Bauser, G.M.; Sauer, K.S. *Extrusion*, 2nd ed.; ASM International: Materials Park, OH, USA, 2006; Volume 200, ISBN 9780871708373.

54. Aoki, S.; Takemura, A. Design and analysis of fractional factorial experiments from the viewpoint of computational algebraic statistics. *J. Stat. Theory Pract.* **2012**, *6*, 147–161. [CrossRef]

55. Pedregosa, F.; Varoquaux, G.; Gramfort, A.; Michel, V.; Thirion, B.; Grisel, O.; Blondel, M.; Prettenhofer, P.; Weiss, R.; Dubourg, V.; et al. Scikit-learn: Machine learning in Python. *J. Mach. Learn. Res.* **2011**, *12*, 2825–2830.

56. Liashchynskyi, P.; Liashchynskyi, P. Grid Search, Random Search, Genetic Algorithm: A Big Comparison for NAS. *arXiv* **2019**, arXiv:1912.06059.

57. Emmert-streib, F.; Dehmer, M. Evaluation of Regression Models: Model Assessment, Model Selection and Generalization Error. *Mach. Learn. Knowl. Extr.* **2019**, *1*, 521–551. [CrossRef]

58. Su, J.; Cheng, Y.; Song, S.; Ma, H.; Wang, W.; Wang, Y.; Zhang, S. Explosion Characteristics and Influential Factors of Coal dust/sodium Chlorate Mixture on Basis of an Explosion Accident in China. *Combust. Sci. Technol.* **2021**, *193*, 1313–1325. [CrossRef]